

Scalable and Conservative Continuous Collision Detection for GPU

David Belgrad
New York University

Marco Attene
IMATI - CNR

Bolun Wang
Beihang University

Daniele Panozzo
New York University

Zachary Ferguson
New York University

Teseo Schneider
University of Victoria

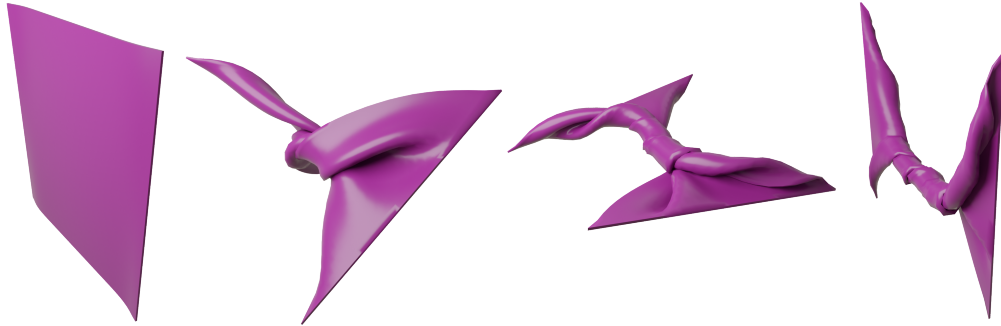


Figure 1: We utilize our scalable continuous collision detection (CCD) algorithm within the simulation of elastic material to detect and prevent collisions [Li et al. 2020]. Here we show one such simulation where we twist a tetrahedralized mat (9K tetrahedra) several times. Our method accelerates both the CCD and the distance computations used throughout the simulation. This leads to a 3× speed-up in the CCD and a 1.1× speed-up overall.

ABSTRACT

We introduce an algorithm for continuous collision detection (CCD) for linearized trajectories designed to be scalable on modern parallel architectures and provably correct when implemented using floating point arithmetic.

We employ a classical two-phase approach, with a broad-phase CCD to quickly filter out primitives having disjoint bounding boxes, and a narrow-phase CCD that establishes whether the remaining primitive pairs actually collide. Our broad-phase algorithm is particularly simple, yet efficient and scalable, thanks to the experimental observation that sweeping along a coordinate axis performs surprisingly well on modern GPUs. For narrow-phase CCD, we re-design the recently proposed interval-based algorithm of Wang et al. [2021] to work on massively parallel hardware.

To evaluate the correctness, scalability, and overall performance of our approach, we introduce a large scale benchmark for broad- and narrow-phase CCD with exact times of impact, and compare our approach with five state-of-the-art methods. We integrate our algorithm with the IPC contact solver, and evaluate its impact on challenging simulation scenarios.

We release the dataset with analytic ground truth, which required over 5 CPU years to be generated, the implementation of all the algorithms tested, our testing framework, and a reference CPU and GPU implementation of our algorithm as an open source project to foster adoption and development of linear CCD algorithms.

1 INTRODUCTION

Continuous collision detection (CCD) is used extensively in graphics, engineering, and scientific computing for the simulation of rigid and deformable objects, and in geometry processing to ensure that self-intersections are not introduced in parameterization or deformation applications. Objects are typically represented by triangle meshes. In this work we focus on the common case where mesh vertices move along linear trajectories. Hence, collision can occur either when an edge hits another edge, or when a vertex hits a triangle [Wang et al. 2021].

CCD is usually divided into two steps: (1) broad-phase, which is a conservative filter that identifies candidate colliding pairs, and (2) narrow-phase, which validates each pair with an accurate and more computationally intensive algorithm. While the narrow-phase is local and involves only a pair of primitives, the broad-phase usually relies on acceleration data structures to prune unnecessary pairs and avoid the quadratic complexity of a brute-force evaluation on all possible pairs. Both problems have been extensively studied in graphics, engineering, and scientific computing in the last three decades (Section 2).

Approximate CCD. CCD algorithms are often used as a building block of contact solvers, which usually introduce contact forces to remove collision between primitives present in a scene. Since the forces are introduced after a collision happens to remove the intersections, these methods do not require a conservative CCD algorithm: small numerical errors in the CCD queries are unlikely

to affect the overall simulation and it is thus common to sacrifice numerical guarantees in the CCD algorithm, favoring approximations that lead to a lower computation cost.

Conservative CCD. Conservative CCD is necessary when numerical errors cannot be tolerated, such as in a new trend of contact models and corresponding simulators [Ferguson et al. 2021; Li et al. 2020, 2021] which guarantee (and also assume), by construction, that no interpenetrations are present in the scene at any moment in time. These algorithms provide a robust and accurate modeling of contact, but are unable to tolerate CCD imprecisions: if a CCD query misses a collision, a self-intersection will appear breaking the assumption of a self-intersection free state, and thus prevents the simulation from terminating. These imprecisions include floating-point rounding errors, which need to be accounted for in a conservative CCD algorithm.

Broad-Phase. The broad-phase of a CCD algorithm usually aims at detecting collision between (axis-aligned) boxes around primitives. Several existing methods simplify the problem by either checking for collisions only at the end of the time interval (i.e., discrete collision detection), or by assuming that only a small fraction of the scene moves. These simplifications allow for faster algorithms; however, they are not realistic in presence of elastic bodies. Many acceleration data structures exist (e.g., hash grids, spatial trees, bounding volumes hierarchies) to avoid checking “far away” boxes, each providing different advantages in different situations. However, most of these structures are complex to parallelize in particular on GPUs where dynamic memory allocation is not an option. Additionally, these structures’ complexity make it hard to verify and ensure correctness when using floating-point computations. In our work, we discovered that the simplest strategy, sweep along the most varying axis, is the most effective on GPUs. The algorithm requires only a parallel sort for the sweep, then every GPU core will compare pairs of boxes. This strategy is not only simple and massively parallel, but it is also trivial to ensure correctness: the only computation performed on the boxes is comparison between floating-point numbers, which is exact.

Narrow-Phase. To the best of our knowledge, the only method providing a conservative exact narrow-phase CCD check for *linear* trajectories is the Tight-Inclusion (TI) CCD of Wang et al. [2021]. Their main idea is to use an interval based root find with floating-point filters to ensure correctness on the result. Unfortunately, TI cannot be directly translated to GPU as it contains several branches, dynamic allocation, and registers. In our work, we redesigned TI to be GPU friendly.

Two-Pronged Evaluation Approach. Validating correctness of algorithms implemented in floating-point is a major challenge, especially when multiple operating systems and architectures are considered, since floating-point computations slightly differ due to either hardware specifics or modern compilers trying to reorder operations to improve performance. This makes it challenging to have a correct code and especially hard to keep it up to date, as compilers and architectures evolve. To provide a way to validate our implementation on a specific system, we provide a large dataset of CCD queries evaluated using exact computations (Section 4)

and we provide a large statistical experimental validation of our method.

Evaluation. We compare our algorithm with five state-of-the-art methods on five different scenes; our overall CCD algorithm (broad and narrow-phase) is up to 20 times faster than the best competing method (Section 5). To show the effectiveness of our acceleration, we integrate our method into IPC [Li et al. 2020] and run several challenging examples showing that our method provides a 3.1 to 11.5× speed-up in CCD and 1.1 to 4.5× total speedup.

Contributions. In our work we introduce a novel CCD pipeline for linearized trajectories. Given two meshes for the start and end of a step, our method returns the time at which the impact occurs. Our pipeline includes the novel parallel GPU and CPU broad-phase algorithm we call Sweep and Tiniest Queue as well as a redesign of the TI algorithm to account for GPU-specific limitations. Additionally, we introduce a dataset of five scenes obtained from different simulator containing between 50 thousands to half a million primitives (i.e., vertex-face and edge-edge). For every successive pair of frames we compute the ground truth Boolean result and time of impact using a symbolic solver [Wolfram Research Inc. 2020]. We use this dataset to validate the output of our system.

2 RELATED WORK

We present an overview of the broad and narrow phase collision detection algorithms that we benchmark in our study, and refer to [Serpa and Rodrigues 2020] for a more complete one for the broad-phase and to [Wang et al. 2021] for narrow-phase collision detection algorithms.

2.1 Datasets

The UNC Dynamic Scene Benchmarks [Curtis et al. 2012] features keyframes from simulation data and is commonly used throughout collision detection works as a source of benchmark data. This dataset covers a variety of simulation methods, materials (e.g., deformable and rigid), and physics (e.g., cloth and fracturing solids). We borrow three scenes (cloth-funnel, cloth-ball, and n-body simulation) from this dataset to test and benchmark our algorithm. Additionally, we provide the ground truth Boolean results and symbolic time of impacts which was not included in the original dataset.

Serpa and Rodrigues [2020] benchmark several classic broad-phase collision detection algorithms. In doing so they provide not only reference implementations of these algorithms but also a benchmarking framework and procedurally generated scenarios. These benchmark scenes focus on simple primitives (e.g., cubes and spheres) in free-fall or undergoing random motion. In contrast with our work, we focus exclusively on triangle meshes. Serpa and Rodrigues [2020] also focus entirely on static collision detection where as our work evaluates broad-phase methods on continuous collision detection scenarios.

Wang et al. [2021] introduced a large scale dataset for narrow-phase CCD algorithms. The dataset is designed to cover common cases extracted from simulation scenarios and challenging degenerate cases. Wang et al. [2021] use the dataset to evaluate the accuracy (the number of false positives), correctness (the number of false

negatives) and efficiency (the average runtime) of different narrow-phase CCD algorithms. However, the large scale dataset proposed by Wang et al. [2021] contains only the queries and the ground truth Boolean results, but not the collision time for each query. In this paper, we propose a new benchmark dataset of over 4M collisions combined with their time of impact (Section 4). This allows us to not only validate the time of impact computed by our method but also evaluate its accuracy.

2.2 Broad-Phase

We discuss the 12 methods benchmarked in [Serpa and Rodrigues 2020] and additionally include the spatial hash data structure used in [Li et al. 2020]. We note that broad phase methods can be used for both static or continuous collision detection by just changing the geometric proxies used: instead of building a proxy, such as a bounding box, around a static object, it is possible to build the proxy around the linearized trajectory in a time-step. Their performance is however very different in these two settings, due to the much larger number of overlaps in the continuous collision detection case.

BF. A simple *CPU parallel brute-force* check where every box in the list is checked against every other box. To avoid any concurrent accesses to the resulting candidates, we use a synchronized vector [Dagum and Menon 1998] and the algorithm is accelerated using AVX instructions. This algorithm is simple, but its complexity is $O(n^2)$, with n the number of primitives: it is not practical for large scenes, but it is viable for smaller ones.

SAP. A serial standard implementation of the *sweep and prune algorithm* [Baraff 1992]: it starts by performing an intersection check between the x -axes of the boxes by sorting the boxes along x . For every x -intersecting box, the algorithm proceeds by checking y and z , every time sorting and pruning the axis. This algorithm improves over the simple brute force as its complexity is $O(n \log(n))$.

GpuSAP. An OpenCL GPU implementation of the SAP algorithm in Bullet 3 [Coulmans and Bai 2019] based on [Liu et al. 2010].

Grid. The scene is divided into voxels (or cells) of uniform size v . The voxel size v is chosen based on a target number of boxes per voxel (we use the default: 200 boxes per voxel). Every input bounding box is assigned to the cells intersecting it. We detect intersections between boxes by iterating over the sparse cells. This algorithm is efficient and easily parallelizable; however, its main disadvantage is the choice of v : a small v will lead to many boxes and an explosion in memory due to duplicate collision candidates, and a large v leads to many boxes inside each cell (e.g., if there is only one voxel the grid reduces to BF). The choice of v is particularly problematic for the large displacements. For instance, if the objects are moving apart, the grid (and the number of boxes) will grow in size, potentially leading to an exploding number.

GSAP. This method is similar to the Grid method but uses a SAP per cell to detect collisions. A small v will result in many duplicate candidates and large memory usage, but, unlike Grid, a large v reduces to SAP and is therefore more efficient than Grid’s BF comparisons.

SH. A parallel CPU implementation of Grid, that encodes the grid implicitly using a *spatial hashing* function. Each candidate box is rasterized in the grid, and for each voxel, a hash value is computed. These hash values are used to store the elements IDs in a hash map (mapping from voxel indices to a vector of element IDs contained inside the voxel). The candidate collisions can then be found by rasterizing the query element and looking up the voxel indices. Our implementation is based on the code from [Li et al. 2020], which has been modified to produce all collision candidates in one parallel loop and include axis-aligned bounding box checks of elements, to make it comparable with the other approaches. This algorithm has the same shortcomings as Grid: a wrong choice of v might lead to either slow performances or excessive memory usage. We use a heuristic for the voxel size equal to two times the maximum of the average edge lengths and the average displacement length. This ensures the average element fits within a single voxel.

GpuGrid. An OpenCL GPU parallel implementation of the Grid algorithm based on Bullet [Coulmans and Bai 2019]. It requires the same delicate choice of v that is even exacerbated as GPUs have less memory than CPUs.

BVH. A *bounding volume hierarchy*. The boxes are divided into two sets: query and target. The target queries are sorted using Morton encoding to optimize spatial locality. The sorted boxes are grouped into pairs, and each pair will form a larger box. By recursively iterating the process, we obtain a *binary tree*, where the root is a box containing the whole space-time scene. Every query box traverses the tree by recursively checking its intersection with the box at the tree’s node until it reaches the leaf. The BVH can be updated “bottom-up” (i.e., if a leaf box grows, it can update its parent until the root), dramatically reducing the update cost in dynamic scenes. We use a *deferred BVH (DBVT-D)* which performs a single tree-tree query.

GpuLBVH. An OpenCL GPU implementation of the Linear BVH in Bullet [Coulmans and Bai 2019]. Similar to the BVH, the tree is organized using Morton encoding. By default, Serpa and Rodrigues [2019] assume a maximum of $18n$ possible intersections, with n input bounding boxes, and discards any successive one. Changing the default size for all our scenes required a trade off between performance for smaller scenes in exchange for more collisions in larger scenes. To avoid this unnecessary shortcoming, which introduces false negatives, we changed the algorithm to process all intersections in an appropriate amount of time: If the list of candidates reaches the maximum, we stop storing them and just count their number. Once we know the total number of candidates, we re-execute the algorithm with the correct preallocated size. We note that this change affects only a few cases where the number of candidates is larger than $18n$.

KDT. An optimized *KD-Tree* designed to handle static scenes based on the efficient implementation in [Serpa and Rodrigues 2019]. The spatial subdivision is designed to adaptively partition the space and have a small number of boxes attached to each cell. We note that when using the automatic box-inflation present in the implementation [Serpa and Rodrigues 2019], the algorithm does not report any collision (i.e. it fails to detect true positives). We thus alter the code to disable this feature and use our own default 1%

inflation, which leads to reasonable results, suggesting that there is a bug in the auto inflation code.

Tracy. The parallel method of Tracy et al. [2009] who builds off the incremental SAP of Baraff [1992] and Cohen et al. [1995] by including the ability to insert AABBs without the need to perform a full sort of the axes.

CGAL. The CGAL implementation of an interval-tree SAP algorithm designed to handle d -dimensional axis-aligned boxes (in our experiments, we use $d = 3$) [Kettner et al. 2016; Zomorodian and Edelsbrunner 2000]. This method works by first performing a SAP on the first axis and then uses range- and interval-trees on the subsequent axes.

2.3 Narrow-Phase

Narrow-phase CCD can be represented as a root finding problem of a function of time. Roots of this function correspond to the point of impact. CCD of linear trajectories without minimal separation equates to finding the roots of a cubic polynomial. Many methods focus on solving these cubic polynomials using numerical methods [Provot 1997]. Provot [1997] introduce the most common strategy of finding a time of coplanarity and then performing an inside check. This idea has since been expanded to solve both rigid [Kim and Rossignac 2003; Redon et al. 2002] and deformable collisions [Hutter and Fuhrmann 2007; Tang et al. 2011].

The down fall of these methods is that they assume infinite precision. When implemented using floating-point numbers, these methods can both miss collisions (false negatives) and report non-existent collisions (false positives).

Alternatively to numerical root-finding algorithms, some propose using inclusion-based root-finding algorithms to determine if a root exists in the co-domain of our function with some tolerance [Redon et al. 2002; Snyder 1992; Snyder et al. 1993; Von Herzen et al. 1990; Wang et al. 2021]. This can either be done using interval arithmetic [Snyder 1992] or by designing custom inclusion functions [Wang et al. 2021]. The latter has the benefit of producing tighter inclusion functions than general interval arithmetic and can be performed in floating-point with specially crafted error bounds. These methods are able to avoid false negatives, but can produce false positives which add extra numerical padding to simulated objects and can result in worse convergence when used in line-search based implicit solvers.

Both Brochu et al. [2012] and Tang et al. [2014] propose exact CCD methods, but despite their claims these methods have been shown to produce both false positives and negatives [Wang et al. 2021]. The only existing method for determining the exact solution is to perform expensive symbolic root finding [Wolfram Research Inc. 2020]. Unfortunately, this is computationally expensive and impractical to use in a simulation pipeline. We use the ground truth generated by this method to verify the results of all queries used in this work.

3 ALGORITHM

Our algorithm, summarized in Algorithm 1, takes as input two triangle meshes M_0, M_1 at time $t = 0$ and $t = 1$ moving along linear trajectories and returns the earliest time of impact t^* ($t^* = \infty$

if there are not collision between M_0 and M_1). The two triangle meshes are represented as a collection of triangles T_i indices and vertex coordinates V_i represented using floating-point numbers. Our parallel algorithm is implemented both on GPU and CPU.

Overview. We first build a set $B = \{b_i\}, i = 1, \dots, k$ of k boxes $b_i = (b_i^m, b_i^M)$ (b_i^m, b_i^M are the min and max corner of the box respectively) around every primitive (triangles, edges, and vertices) on M_0 and M_1 . On GPU we represent them in *single* precision while ensuring that every input (in double precision) is *exactly* contained in its box b_i (Section 3.1). This phase is fast and takes around 10% of the runtime (Figure 2).

Then we pass B to our broad phase algorithm to discard any far away candidate (Section 3.2). The broad phase produces a set of n candidates intersection $C = \{(l_i, r_i) | 1 \leq i \leq n\}$, where every pair (l_i, r_i) indicates that the primitives in the boxes b_{l_i} and b_{r_i} potentially intersect. This stage takes about 50% of the runtime (Figure 2).

Finally, to obtain the time of impact t^* , we run a parallel version of TI using the collision candidates C and the input meshes M_0 and M_1 (Section 3.3). The core idea is the same as in [Wang et al. 2021], but we redesigned the algorithm avoiding recursion and using a worker queue paradigm to make it GPU parallelizable. This stage accounts for 30% of the runtime on average (Figure 2). Note that, on GPU, we execute the narrow-phase using the same precision as the input (e.g., double precision for all our experiments)¹.

Algorithm 1 Overview of our CCD algorithm.

```

1: function CCD( $M_0, M_1$ )
2:    $B \leftarrow \text{BUILD\_BOXES}(M_0, M_1)$                                  $\triangleright$  CPU, Section 3.1
3:    $C \leftarrow \text{BROAD\_PHASE}(B)$                                      $\triangleright$  GPU, Section 3.2
4:    $t^* \leftarrow \text{NARROW\_PHASE}(C, M_0, M_1)$                        $\triangleright$  GPU, Section 3.3
5:   return  $t^*$ 
6: end function

```

3.1 Construction of the Boxes

To construct a *tight* single precision box $b = (b^m, b^M)$ around a primitive (i.e., a triangle, edge, or vertex) we first compute the extend of the box b^m, b^M in double precision using the min and max of the coordinates of the primitive. For instance, for a triangle, b^m is the minimum of the x, y, z -coordinates of the three vertices. To *conservatively* convert b^m in single precision, for each coordinate (e.g. x) we first round b_x^m to its nearest single precision value and check if $b_x^m < b_x^M$, in case it is not, we decrease b_x^m to its previous representable single precision value using the function `nextafterf`². The procedure for b^M is similar. When running our algorithm on GPU, we need to copy the boxes on the device; in our experiments this time, B2G, is negligible (Figure 2).

3.2 Broad-Phase

Our Sweep and Tiniest Queue (STQ) algorithm is based on the (surprising) observation that brute-force checking all possible pairs is

¹Modern consumer GPUs have very limited support for double computation, but this is not an issue for our purposes, as the narrow-phase is memory bound and the lower number of double-precision ALUs does not affect the algorithm performance.

²<https://en.cppreference.com/w/c/numeric/math/nextafter>



Figure 2: Cutoff of the runtime for every scene for our method on the different architectures. NP runs the narrow phase, V2G copies the vertices to the GPU; SO splits the queries into vertex-face and edge-edge; BP is the broad phase; CD constructs the data list; B2G copies the boxes to the GPU; and CB constructs the boxes. Section 5 details the different architectures.

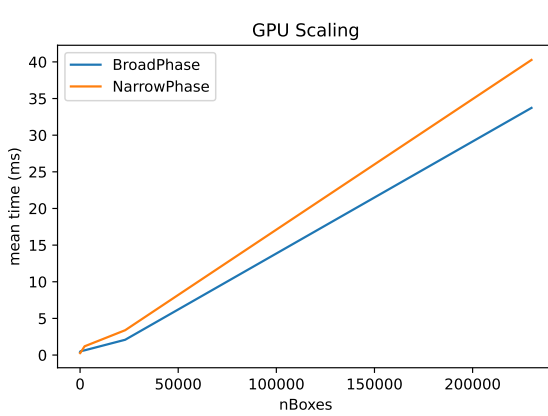


Figure 3: Run time of our algorithm with respect to the number of queries. To generate varying number of queries, we select a random sub-sample of all possible boxes from the last 10 frames of Rod-Twist.

not only easy to parallelize, but very fast on modern architectures due to their memory layout and large number of ALUs, which favors heavier computation with a structured memory access. Unfortunately, this simple approach has a runtime quadratic with respect to the number of pairs and cannot be applied to large scenes. To overcome this limitation we borrow ideas from the Sweep and Prune algorithm [Baraff 1992; Cohen et al. 1995] to limit the average complexity of our algorithm (Figure 3).

Algorithm. Our STQ starts by computing the variance σ of the boxes' centers B_C and finding the most varying axis a (line 4) [Liu et al. 2010]. We then sort the boxes B along the axis a and initialize a queue Q_i that will hold pairs of boxes that overlap on the a -axis. Since a is the axis of maximum variance this will lead to the smallest possible queue among the three axes if the data is uniformly distributed.

In the first step, for every box b_i we check if it intersects its next box b_{i+1} along the a -axis; if it does we append the pair (b_i, b_{i+1}) to Q_i (line 8).

Then STQ extracts a pair (b_i, b_j) from Q_i and check if it intersects in the remaining two axes a^c (line 17). If they do, we append the pair to the output C (global). Finally we add the pair (b_i, b_{j+1}) to an output queue Q_o if (b_i, b_{j+1}) intersects along the a -axis (line 21, Figure 4).

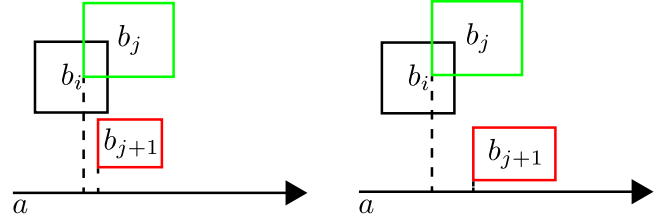


Figure 4: The boxes b_i , b_j , and b_{j+1} are sorted along the axis a . Since b_i and b_j intersect, we append the pair to C and check b_{j+1} . If b_{j+1} intersects b_i on the axis a (left) we append the (b_i, b_{j+1}) to Q_o , if not (right) we discard the pair.

Implementation Remarks. We remark that the STQ algorithm creates queues with *at most* $k - 1$ elements, as each pass on Q_i pushes at most one pair. Additionally, as not all pairs are always added, the sizes are monotonically decreasing. On GPU, we exploit this observation to pre-allocate the correct queue-size and guarantee that we will always have the necessary space. To efficiently parallelize STQ on GPU we exploit shared memory per thread block. In our experiments, the most efficient strategy consists of splitting the sorted boxes B' into m blocks containing 32 queries each (i.e., $m = k/32$). Since a warp consists of 32 threads, choosing a smaller number will introduce unnecessary branching. Using larger thread blocks can lead to more imbalanced workloads and longer runtime of branching in the code. The GPU thread block-scheduler performs well even with a larger grid size of thread blocks.

When running our algorithm on GPU, we need to prepare the data for the narrow-phase; this requires:

- (1) splitting the set C into edge-edge and vertex-face cases (SO),
- (2) transforming the pairs in C into narrow-phase data (CD),
- (3) coping the vertex coordinates to the device (V2G).

Similar to copying the boxes to GPU these intermediate stages are negligible (Figure 2).

3.3 Narrow-Phase

Since our algorithm builds upon [Wang et al. 2021], we first provide a self-contained overview of the original algorithm.

Summary of [Wang et al. 2021]. The algorithm uses interval arithmetic to detect collisions. It starts by constructing the interval $I = I_t \times I_{uv} \subseteq [0, 1]^3$, where $I_t = [0, 1]$ is the time interval and I_{uv} is the parameterization of the space. For a point-face query

Algorithm 2 Overview of the broad-phase.

```

1: function BROAD_PHASE( $B$ )
2:    $B_C \leftarrow \{c = (b^m + b^M)/2 | b \in B\}$             $\triangleright$  Box centers
3:    $\sigma \leftarrow \sigma(B_C)$                                  $\triangleright$  Variance of the boxes centers
4:    $a \leftarrow \text{argmax}_{i=\{x,y,z\}} \sigma^i$ 
5:    $a^c \leftarrow \{x, y, z\} \setminus a$ 
6:    $B' \leftarrow \text{SORT}(B, \text{ORDER}(a, B_C))$             $\triangleright$  in parallel
7:    $Q_i \leftarrow \{\}$ 
8:   for all  $i \in [1, \dots, k-1]$  do
9:     if  $b_i^a \cap b_{i+1}^a \neq \emptyset$  then
10:       $Q_i \leftarrow Q_i \cup (b_i, b_{i+1})$ 
11:    end if
12:   end for
13:
14:   while  $Q_i \neq \emptyset$  do
15:      $Q_o \leftarrow \{\}$ 
16:     for all  $(b_i, b_j) \in Q_i$  do
17:       if  $b_i \cap b_j \neq \emptyset$  then
18:          $C \leftarrow C \cup (b_i, b_j)$ 
19:       end if
20:       if  $b_i^a \cap b_{j+1}^a \neq \emptyset$  then
21:          $Q_o \leftarrow Q_o \cup (b_i, b_{j+1})$ 
22:       end if
23:     end for
24:      $Q_i \leftarrow Q_o$ 
25:   end while
26:   return  $C$ 
27: end function
28:
29: function ORDER( $a, c_i, c_j$ )
30:   return  $c_i^a < c_j^a$                                  $\triangleright$  Order is given by the axis  $a$ 
31: end function

```

$I_{uv} = \{(u, v) \mid 0 \leq u, v \leq 1 \wedge u + v \leq 1\}$, where u and v are the triangle's barycentric coordinates. For an edge-edge query $I_{uv} = [0, 1]^2$, where u and v are the first and second segment parameter. Using I , the algorithm defines the box $B = B_F(i)$ [Wang et al. 2021, (4)] that, if it intersect with a tolerance box C_ϵ [Wang et al. 2021, (5)], determines if the interval I contains a root or not. In case it does, the algorithm recursively splits I into two subintervals [Wang et al. 2021, Algorithm 2] until they are either too small or completely contained in C_ϵ .

Algorithm. The method of Wang et al. [2021] can be trivially parallelized on a CPU, by adding a parallel loop around the candidates C . This strategy works well, but it is unfortunately not compatible with a GPU architecture, which for good performance requires all threads to perform exactly the same operations and have similar memory access patterns. This is not the case for Wang et al. [2021], as each query requires a different number and type of subdivisions. To overcome this limitation, we note that the core of the algorithm processes intervals and not queries (Algorithm 3): we can thus parallelize over interval splits instead than on queries.

This observation leads to performing the same operations on every thread independently from the candidate³.

We start by constructing, for every collision candidate C , the initial interval $I = [0, 1]^3$ (line 2) and append them to the input queue Q_i . We then process in parallel all intervals in Q_i and produce and output intervals' queue Q_o (line 6). At the end, we swap the roles of the two queues (line 15) and continue alternating until Q_o is empty.

Time of Impact. We modified how we process a single interval (line 20) with respect to [Wang et al. 2021] to account for the time of impact. We first check if I_t^l (i.e., left hand-side of the time interval of I) is larger than the current time of impact t^* . In this case I can safely be skipped (line 22). Then we proceed as in [Wang et al. 2021] and, if the box B constructed from I does not intersect C_ϵ , I can be discarded as it does not contain a root (line 26). Finally, if the width $w(I)$ of I is smaller than a user provided tolerance δ (or if B is contained in C_ϵ), we report collision and return I_t^l (29). If it is not the case, we split I into a left I^l and right I^r interval and return the current time-of-impact as optimal.

Discussion. The algorithm has only two necessary synchronizations: 1) the update of t^* and 2) appending intervals to Q_o . We update t^* using a mutex as atomicMin does not support floating-point numbers. To efficiently append intervals we keep track of the size of Q_o and use atomicAdd to increase the size counter when appending new elements.

4 DATASET GENERATION

Our dataset is composed of five simulated scenes (Figure 5 top row) and the corresponding ground truth data for continuous collisions between frames. From the UNC Dynamic Scene Benchmark [Curtis et al. 2012], we include two co-dimensional cloth simulations with a large number of self collisions (Cloth-Ball and Cloth-Funnel) and a simulation of a large number of rigid and deformable spherical bodies (N-Body). We also include two elastodynamic scenes featuring large compression and nonlinear buckling simulated using the method of Li et al. [2020] (Armadillo-Rollers and Rod-Twist).

Ground Truth. Differently from all other datasets for CCD, we generate ground truth for each successive pair of frames from each scene, using a combination of symbolic computation and conservative filtering. This is done by first enumerating all possible collision pairs (collision candidates) through a brute-force approach. We only consider point-triangle and edge-edge pairs as these pairs capture the first collisions between triangles [Provot 1997]. Furthermore, we ignore points that are vertices of the triangles and edges that share a common endpoint as these are trivially colliding. For each collision candidate, we determine if the pair collides using the provably conservative CCD of Wang et al. [2021]. While this CCD algorithm is guaranteed to not have false negatives, it may produce false positives. To eliminate false positives, we find exact solutions of the CCD query using the symbolic solver in Mathematica [Wolfram Research Inc. 2020]. While we could skip the middle step and

³An additional subtle benefit of this algorithm is that it makes the GPU kernel shorter, reducing the number of registers used, which is a common performance bottleneck on GPUs, where each streaming multiprocessor (SM) has a very small pool of registers available.

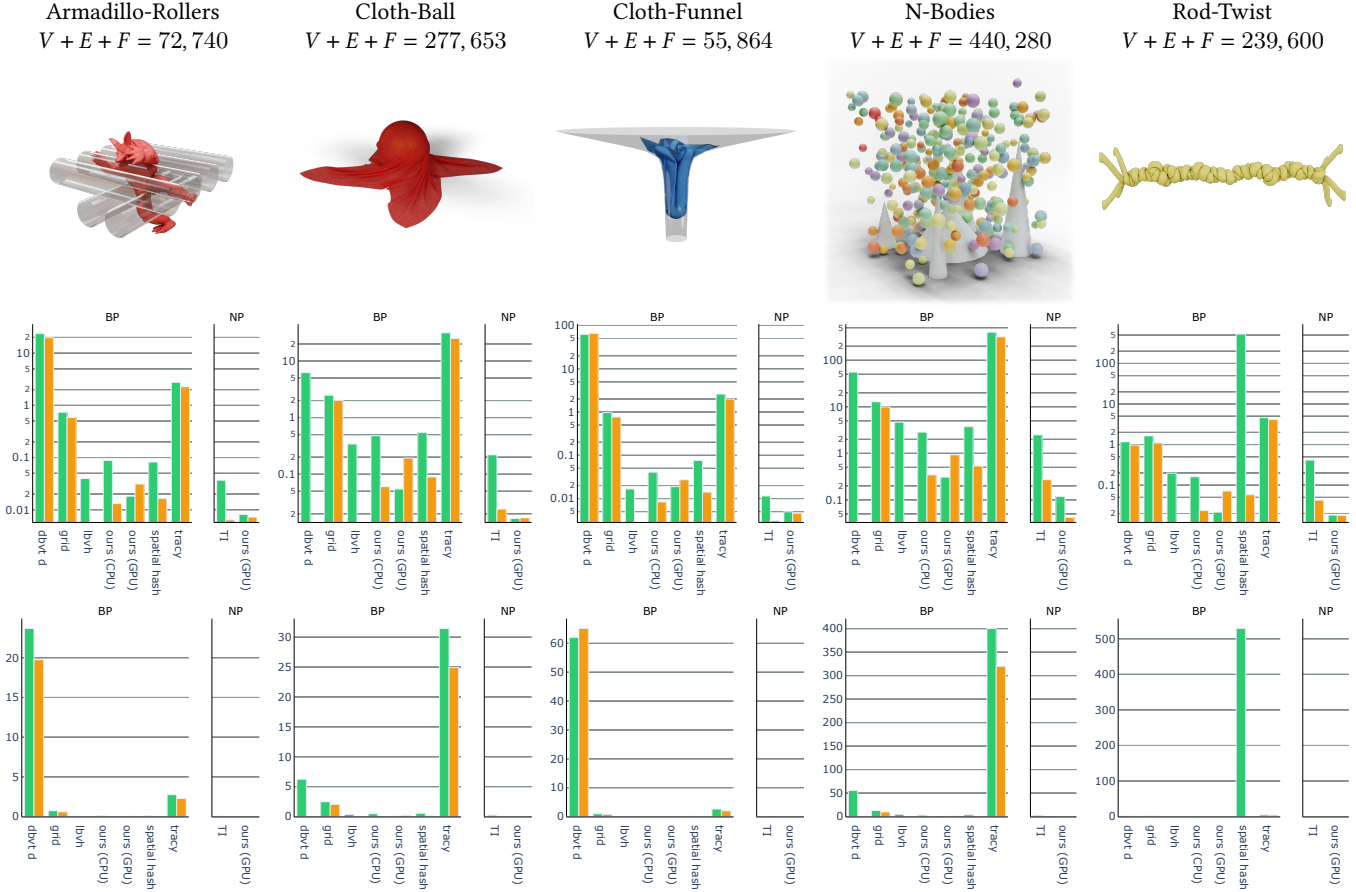


Figure 5: Log (top) and normal (bottom) bar charts of the timings for every scene. The green colors shows the performances for the consumer architectures (CPU1 and GPU1), while orange is for the professional ones (CPU2 and GPU2).

directly use the symbolic CCD this would be prohibitively slow, as the symbolic solvers take several seconds per query. Instead, the method of Wang et al. [2021] quickly filters the majority of the collision pairs, leaving a smaller number of candidates to validate with the symbolic solver.

Time of Impact Expressions. In addition to the Boolean ground truth we also include the symbolic expressions for the valid roots (as Wolfram Language MX files). It is necessary to save the symbolic expressions (instead of a real or rational number) as they may include operators and functions that cannot be evaluated exactly (e.g., square roots). These expressions are later used to validate our time of impact and evaluate its accuracy (see Section 5.3). In total this includes over 3.3M edge-edge and 728K vertex-face contacts. For reproducibility, we provide scripts to rerun the validation on other architectures and compilers.

5 RESULTS

We run all CPU methods on two CPUs: CPU1 a consumer architecture (Intel®Core(TM) i7-5930K CPU @ 3.5 GHz) and CPU2 a professional CPU (AMD Ryzen Threadripper PRO 3995WX 64-Cores @ 2.7 GHz) and two GPU: GPU1 a gaming card (Nvidia

3080 Ti) and GPU2 a professional card (NVidia v100). For every CPU run we limit the number of threads to 12. We note that for many computation CPU2 behaves like a GPU⁴ but costs around ten times more.

5.1 Comparison

For each broad-phase algorithm, we compare the list of candidates with the ground truth data. We report the average running time for correct implementations (the additional material reports the timings of all methods). We note that all methods detect similar number of candidates. The LBVH method provides a function to update the data structure with new positions instead of rebuilding it from scratch at every frame, which we use in our experiments. For all other methods, the acceleration data structure is rebuilt at each frame. The results are summarized in Figure 5. For the narrow-phase we compare only with TI [Wang et al. 2021] as it is the only correct algorithm. For each narrow-phase algorithm, we only record the time of impact for the whole time-step.

The performance of the broad phase methods are mostly independent from the scene: ours, LBVH, and SH are among the fastest

⁴<https://opendata.blender.org/>

Algorithm 3 Overview of the narrow-phase.

```

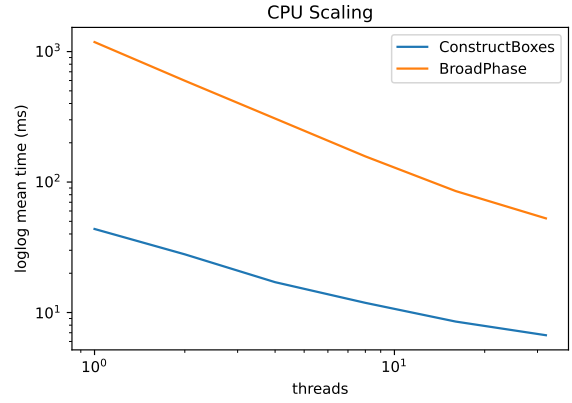
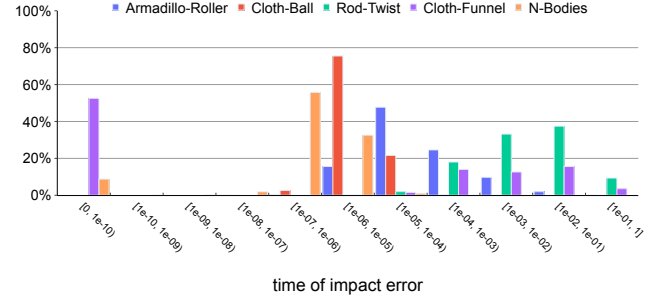
1: function NARROW_PHASE( $C, M_0, M_1$ )
2:    $Q_i \leftarrow \text{BUILD\_INTERVALS}(C, M_0, M_1)$ 
3:    $t^* \leftarrow 1$ 
4:   while  $Q_i \neq \emptyset$  do
5:      $Q_o \leftarrow \emptyset$ 
6:     for all  $I \in Q_i$  do                                 $\triangleright$  In parallel
7:        $t^*, I^l, I^r \leftarrow \text{PROCESS\_INTERVAL}(I, t^*)$ 
8:       if  $I^l \neq \emptyset$  then
9:          $Q_o \leftarrow Q_o \cup I^l$ 
10:      end if
11:      if  $I^r \neq \emptyset$  then
12:         $Q_o \leftarrow Q_o \cup I^r$ 
13:      end if
14:    end for
15:     $Q_i \leftarrow Q_o$ 
16:   end while
17:   return  $t^*$ 
18: end function
19:
20: function PROCESS_INTERVAL( $I, t^*$ )
21:    $t \leftarrow I^l_t$ 
22:   if  $t \geq t^*$  then                                 $\triangleright$  Current interval is after  $t^*$ 
23:     return  $t^*, \emptyset, \emptyset$ 
24:   end if
25:    $B \leftarrow B_F(I)$ 
26:   if  $B \cap C_\epsilon = \emptyset$  then                   $\triangleright$   $I$  does not have collision
27:     return  $t^*, \emptyset, \emptyset$ 
28:   end if
29:   if  $w(B) < \delta$  or  $B \subseteq C_\epsilon$  then       $\triangleright$  Collision found
30:     return  $t, \emptyset, \emptyset$ 
31:   end if
32:    $I^l, I^r \leftarrow \text{SPLIT}(I)$                        $\triangleright$   $I$  gets refined
33:   return  $t^*, I^l, I^r$ 
34: end function

```

methods. Our method on GPU is between 10 and 16 times faster than LBVH on large scenes (Cloth-Ball, N-Bodies, and Rod-Twist) and has a comparable time for smaller ones. On CPU our method has similar performance to the spatial hash, however it does not require to tweak the cell size.

The narrow phase on GPU is faster than the broad phase (just barely for the Rod-Twist and 9 times for the N-Bodies); on CPU the two phases are more comparable (NP is 3 times slower on Rod-Twist and 3 times faster on Cloth-Funnel). The difference comes from the fact that the NP on GPU is up to 80 faster than CPU, while the BP peaks at 10 times faster. As expected for our method CPU2 (orange) has similar performance to GPU1 (green).

Overall our GPU algorithm is up to 20 times faster for larger scenes than the best existing combination (LBVH for BP and CPU parallel TI) on consumer hardware (3 for Armadillo-Rollers, 10 for Cloth-Ball, 1.6 for Cloth-Funnel, 22 for N-Bodies, and 17 Rod-Twist).

**Figure 6:** Strong scaling of our method for the last 10 frames of Rod-Twist.**Figure 7:** Using the symbolic ground truth for the time of impact we compute an error per query per scene and plot them as a histogram in log scale. The error is computed as the absolute difference between the earliest root reported by the symbolic root finder and our code (the error is approximately computed using 128bits of precision). All time of impacts computed by our method are verified symbolically to be less than the ground truth.

5.2 Scaling

To assess the scalability of our method we run the last ten frames of Rod-Twist on CPU2 varying the number of threads from 1 to 32 (Figure 6). Our algorithm scales well with respect to the number of threads: with 8 threads the BP is 7.5 times faster and it gets to 22 times faster with 32 threads. Constructing the boxes scales worst: it is just 3.7 times faster with 8 threads and 6.5 for 32.

5.3 Time of Impact Validation and Accuracy

Using the time of impact expressions discussed in Section 4, we both validate our computed time of impacts occur before the ground truth and compute an error for the roots. The results of this study are presented in Figure 7. The average error for over all queries is ~ 0.0023 with a standard deviation of ~ 0.018 and a median error of $\sim 1.03 \times 10^{-6}$. We note that this distribution varies between scenes (e.g., cloth-ball has an average error of $\sim 8.33 \times 10^{-6}$ compared to

Scene	# Verts	# Tets	CCD Time (s)		Total Time (s)		CCD Speed-Up	Total Speed-Up
			SH+TI	Ours	SH+TI	Ours		
Sliding Spike	5	2	0.002	0.03	0.05	0.70	0.08x	0.08x
Spikes	5	2	0.003	0.04	0.08	0.65	0.08x	0.12x
Spike and Wedge	5	2	0.003	0.05	0.07	0.69	0.07x	0.10x
Spike in Crack	5	2	0.37	0.62	4.44	7.01	0.60x	0.63x
Sliding Wedge	6	3	0.00	0.03	0.07	0.80	0.07x	0.09x
Wedges	6	3	0.87	0.08	6.69	1.36	11.54x	4.94x
Internal Edges	8	6	0.57	0.30	6.10	2.64	1.88x	2.31x
5 Cubes	40	30	4.51	0.43	40.98	9.11	10.61x	4.50x
Mat-Twist	3200	9126	7.92	2.60	2567.06	2368.87	3.05x	1.08x
Mat-Knives	3200	9126	4.15	0.92	329.46	311.76	4.53x	1.06x

Table 1: Performance of our new CCD and broad phase for the unit tests of Erleben [2018] in [Li et al. 2020, Figure 11], the five cube stack, mat-twist, and mat-knives simulations. For tiny scenes the overhead of our method worsens performance, but in general leads to a performance increase in both the CCD and simulation as a whole. For larger scenes, the bottleneck shifts to the linear solves and Hessian matrix assembly leading to a smaller overall improvement of running time.

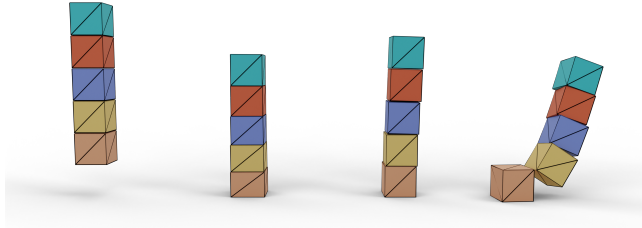


Figure 8: Several frames of the five-cube stack example. The whole scene has only 30 tetrahedra and is therefore CCD bound.

~0.032 for rod-twist). This indicates a dependency between the types of contact and the accuracy of the time of impact.

The error of roots can be easily reduced by incorporating a convergence tolerance on the time domain interval in the narrow-phase. The downside of this would be that it could increase the computational time of the narrow-phase. This choice of accuracy versus runtime is best determined by a user’s chosen application of our CCD.

6 SIMULATIONS

We utilize our GPU CCD algorithm inside the IPC algorithm [Li et al. 2020] implemented in PolyFEM [Schneider et al. 2019] by running several simulation on CPU2 with 8 threads for the simulation and GPU1 for the CCD. We note that IPC requires computing the distances between primitives at the beginning of every time step, which we accelerate using our STQ broad phase algorithm. We run all the unit tests of Erleben [2018] presented in [Li et al. 2020, Figure 11] using the original implementation (that use spatial hash for broad phase and the parallel TI) and compare with our method (Table 1).

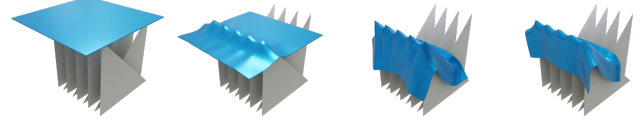


Figure 9: Several frames of a codimensional simulation. The mat has 9K tetrahedra, while the codimensional triangles are not deformable.

We run the five-cube stack example (Figure 8) that contains several resting contacts. Similarly to the unit tests, as the meshes are extremely coarse, when using our method the simulation is 4.5x faster. When using denser meshes (Figure 1 has 9K tetrahedra) and the elastic deformations become more challenging, the non-linear elastic solver dominates the IPC runtime and the speedup provided when using our method becomes less prominent; only 8% times faster overall. Our method naturally support CCD between codimensional object (Figure 9); for this scene we again see similar speedups.

6.1 Avoiding a Time of Impacts Equal to Zero

An important caveat of using a conservative CCD method inside the IPC algorithm is that it should not produce a time of impact t^* of zero. A t^* of zero would stop the non-linear solver because IPC uses the t^* to determine the maximum step-size allowable inside the implicit time-stepping optimization. Additionally, IPC guarantees every step results in an intersection-free state, so t^* cannot be zero (i.e., not initially intersecting).

To avoid a zero t^* , we make slight modifications to Algorithm 1 and 3 (Appendix A). As part of the strategy to avoid $t^* = 0$, the IPC algorithm uses a minimum separation in the CCD to prevent taking a step that results in parts exactly touching. We choose the minimum separation relative to the initial distance between the query’s primitives (0.8x in all our experiments). To implement minimum separation CCD, we use the same strategy as TI [Wang et al. 2021]: we enlarge the box C_ϵ by the minimum separation distance.

7 CONCLUSION

We introduce a novel, scalable CCD algorithm combining broad and narrow phase collision detection. Our algorithm is provably conservative and our implementation has been tested on multiple combinations of recent operating systems and hardware architectures. Our algorithmic contribution specifically targets parallel architectures with high memory bandwidth (and high latency), which have very different requirements than traditional serial architectures. Our algorithm scales well to GPU hardware: a NVidia 3080 Ti GPU (MSRP ~1.2K USD) achieves a speed comparable to a CPU server chip with 64 cores/128 threads (MSRP ~10K USD). We believe that our GPU algorithm could be extended to run on multi-GPU. Our preliminaries experiments show that the broad phase becomes 2.3 times faster when using 4 GPUs for the N-Bodies scene.

While the correctness of our algorithm is provable assuming infinite precision [Baraff 1992; Cohen et al. 1995], certifying that our

implementation is correct, with computation performed with floating point numbers, is very challenging. The correctness will heavily depend on the hardware used and the compiler, which evolve over time. Our dataset provides a way to check for correctness of CCD codes on different settings, and while passing the benchmark is not a formal proof of correctness, we believe it is a realistic and practical approach to evaluate the conservativeness of our implementation. It helped us design our algorithm, and using it we found counter-examples for other CCD codes (Additional material). The benchmark is easy to extend, and we plan to keep it up to date and add to it more scenes and challenging queries in the next years.

When integrated with the state of the art solver IPC, our approach reduces the overall simulation time, which we believe is of practical relevance to the graphics and simulation community. Our implementation will be released on GitHub with the MIT license, to foster its adoption in academia and in industry.

REFERENCES

David Baraff. 1992. *Dynamic simulation of non-penetrating rigid bodies*. Technical Report. Cornell University.

Tyson Brochu, Essex Edwards, and Robert Bridson. 2012. Efficient geometrically exact continuous collision detection. *ACM Transactions on Graphics* 31, 4, Article 96 (July 2012), 7 pages.

Jonathan D. Cohen, Ming C. Lin, Dinesh Manocha, and Madhav Ponamgi. 1995. I-COLLIDE: An Interactive and Exact Collision Detection System for Large-Scale Environments. In *Proceedings of the 1995 Symposium on Interactive 3D Graphics* (Monterey, California, USA) (I3D '95). Association for Computing Machinery, New York, NY, USA, 189–ff.

Erwin Coumans and Yunfei Bai. 2016–2019. PyBullet, a Python module for physics simulation for games, robotics and machine learning. <http://pybullet.org>.

Sean Curtis, Russ Gayle, Naga Govindaraju, Ilknur Kabul, Ming Lin, Simon Pabst, Stephane Redon, Avneesh Sud, Min Tang, Sung-eui Yoon, Jieyi Zhao, and Dinesh Manocha. 2012. UNC Dynamic Scene Benchmarks. <http://gamma.cs.unc.edu/DYNAMICB>.

Leonardo Dagum and Ramesh Menon. 1998. OpenMP: an industry standard API for shared-memory programming. *Computational Science & Engineering, IEEE* 5, 1 (1998), 46–55.

Kenny Erleben. 2018. Methodology for Assessing Mesh-Based Contact Point Methods. *ACM Transactions on Graphics* 37, 3, Article 39 (July 2018), 30 pages.

Zachary Ferguson, Minchen Li, Teseo Schneider, Francisca Gil-Ureta, Timothy Langlois, Chenfanfu Jiang, Denis Zorin, Danny M. Kaufman, and Daniele Panozzo. 2021. Intersection-free Rigid Body Dynamics. *ACM Transactions on Graphics (Proceedings of SIGGRAPH)* 40, 4, Article 183 (2021).

Marco Hutter and Arnulph Fuhrmann. 2007. Optimized continuous collision detection for deformable triangle meshes. (July 2007).

Lutz Kettner, Andreas Meyer, and Afra Zomorodian. 2016. Intersecting Sequences of dD Iso-oriented Boxes. https://doc.cgal.org/latest/Box_intersection_d/index.html

Byungmoon Kim and Jarek Rossignac. 2003. Collision prediction for polyhedra under screw motions. *Proceedings of the Eighth ACM Symposium on Solid Modeling and Applications*, 4–10.

Minchen Li, Zachary Ferguson, Teseo Schneider, Timothy Langlois, Denis Zorin, Daniele Panozzo, Chenfanfu Jiang, and Danny M. Kaufman. 2020. Incremental Potential Contact: Intersection-and Inversion-Free, Large-Deformation Dynamics. *ACM Transactions on Graphics (Proceedings of SIGGRAPH)* 39, 4, Article 49 (July 2020), 20 pages.

Minchen Li, Danny M. Kaufman, and Chenfanfu Jiang. 2021. Codimensional Incremental Potential Contact. *ACM Transactions on Graphics (Proceedings of SIGGRAPH)* 40, 4, Article 170 (2021).

Fuchang Liu, Takahiro Harada, Youngeun Lee, and Young J Kim. 2010. Real-time Collision Culling of a Million Bodies on Graphics Processing Units. *ACM Transactions on Graphics* 29, 6 (Dec. 2010), 1–8.

Xavier Provot. 1997. Collision and self-collision handling in cloth model dedicated to design garments. In *Computer Animation and Simulation*. Springer, 177–189.

Stephane Redon, Abderrahmane Kheddar, and Sabine Coquillart. 2002. Fast Continuous Collision Detection between Rigid Bodies. *Computer Graphics Forum* 21 (May 2002).

Teseo Schneider, Jérémie Dumas, Xifeng Gao, Denis Zorin, and Daniele Panozzo. 2019. Polyfem. <https://polyfem.github.io/>.

Ygor Rebouças Serpa and Maria Andréia Formico Rodrigues. 2019. Flexible use of temporal and spatial reasoning for fast and scalable CPU broad-phase collision detection using KD-Trees. In *Computer Graphics Forum*, Vol. 38. Wiley Online Library, 260–273.

Ygor Rebouças Serpa and Maria Andréia Formico Rodrigues. 2020. Broadmark: A Testing Framework for Broad-Phase Collision Detection Algorithms. *Computer Graphics Forum* 39, 1 (2020), 436–449.

John M. Snyder. 1992. Interval Analysis for Computer Graphics. *Computer Graphics (Proceedings of SIGGRAPH)* 26, 2 (July 1992), 121–130.

John M. Snyder, Adam R. Woodbury, Kurt Fleischer, Bena Currin, and Alan H. Barr. 1993. Interval Methods for Multi-Point Collisions between Time-Dependent Curved Surfaces. In *Proceedings of the 20th Annual Conference on Computer Graphics and Interactive Techniques* (Anaheim, CA) (SIGGRAPH '93). Association for Computing Machinery, New York, NY, USA, 321–334.

Min Tang, Dinesh Manocha, Sung-eui Yoon, Peng du, Jae-Pil Heo, and Ruofeng Tong. 2011. VolCCD: Fast continuous collision culling between deforming volume meshes. *ACM Transactions on Graphics* 30 (Jan. 2011), 111.

Min Tang, Ruofeng Tong, Zhendong Wang, and Dinesh Manocha. 2014. Fast and Exact Continuous Collision Detection with Bernstein Sign Classification. *ACM Transactions on Graphics* 33 (Nov. 2014), 186:1–186:8, Issue 6.

Daniel J Tracy, Samuel R Buss, and Bryan M Woods. 2009. Efficient large-scale sweep and prune methods with AABB insertion and removal. In *2009 IEEE Virtual Reality Conference*. IEEE, 191–198.

Brian Von Herzen, Alan H. Barr, and Harold R. Zatz. 1990. Geometric Collisions for Time-Dependent Parametric Surfaces. In *Proceedings of the 17th Annual Conference on Computer Graphics and Interactive Techniques* (Dallas, TX, USA) (SIGGRAPH '90). Association for Computing Machinery, New York, NY, USA, 39–48.

Bolun Wang, Zachary Ferguson, Teseo Schneider, Xin Jiang, Marco Attene, and Daniele Panozzo. 2021. A Large Scale Benchmark and an Inclusion-Based Algorithm for Continuous Collision Detection. *ACM Transactions on Graphics* (2021).

Wolfram Research Inc. 2020. *Mathematica* 12.0. <http://www.wolfram.com>

Afra Zomorodian and Herbert Edelsbrunner. 2000. Fast Software for Box Intersections. In *Proceedings of the Sixteenth Annual Symposium on Computational Geometry* (Clear Water Bay, Kowloon, Hong Kong) (SCG '00). Association for Computing Machinery, New York, NY, USA, 129–138.

A ZERO TIME OF IMPACT AND MINIMUM SEPARATION

To avoid $t^* = 0$, we make slight modifications to Algorithm 1 and 3. In IPC, if Algorithm 1 return $t^* = 0$ we perform the narrow-phase again but set the minimum separation to 0 and enable a no zero ToI strategy.

This no zero ToI strategy dictates that if $I_t^l = 0$, I should always be split (ignoring user tolerances and maximum number of splits). We note that under floating-point division this split might not be possible, but this has not been encountered in practice and would most likely require a degenerate case involving tiny distances (which IPC does a good job of preventing thanks to its barrier potential method of handling contacts). In the end, because minimum separation was disabled, the resulting t^* is multiplied by a scaling factor less than 1 to avoid exactly touching after the step (we use 0.8 in our examples).